Transportation Research Part C 145 (2022) 103932

Contents lists available at ScienceDirect

Transportation Research Part C

journal homepage: www.elsevier.com/locate/trc

Quasi revenue-neutral congestion pricing in cities: Crediting drivers to avoid city centers

Ye Li [a,b], Mohsen Ramezani [a,*]

[a] The University of Sydney, School of Civil Engineering, Sydney, Australia
[b] Beijing Key Laboratory of Traffic Engineering, Beijing University of Technology, Beijing, China

ARTICLE INFO

Keywords:
Network fundamental diagram
Routing
Receding horizon
Learning-based model predictive control
Machine learning

ABSTRACT

This paper introduces a predictive congestion pricing method in cities wherein the tolls alter from region to region. We consider a large urban network is partitioned into multiple regions each with a well-defined Macroscopic Fundamental Diagram (MFD) where multiple routes exist between each origin and destination regions. The proposed cordon pricing method is designed to (i) minimize vehicles' total time spent in the network and (ii) aim for a revenue-neutral tolling. A controller based on model predictive control (MPC) approach is proposed to determine the (possibly negative) optimal time- and region-varying tolls. The MPC controller comprises a regional MFD-based traffic model with no need of destination information and a long-short term memory neural network (LSTM-NN) to obtain an accurate estimation of inter-region transfer flows. Results of numerical experiments indicate the effectiveness of the proposed congestion pricing method to achieve the two objectives simultaneously, compared with No toll and reactive feedback controllers.

1. Introduction

1.1. Background and motivation

With rapid growth of urbanization, the number of vehicles has expanded expeditiously, which leads to increasingly detrimental traffic congestion in cities. Therefore, several effective traffic management approaches have been developed and applied at the network level to alleviate pockets of congestion. The introduction of network macroscopic fundamental diagram (MFD) has enabled promising directions for the network-level systematic congestion management at a very low computational cost. Examples include congestion pricing (Daganzo and Lehe, 2015; Chen et al., 2021; Gu and Saberi, 2021), perimeter flow control (Aalipour et al., 2018; Mohajerpoor et al., 2020; Li et al., 2021; Sirmatel and Geroliminis, 2021; Li et al., 2021), route guidance (Yildirimoglu et al., 2015, 2018; Batista et al., 2021), ramp metering (Haddad et al., 2013; Han et al., 2020), and multi-modal operation control, e.g. taxis or public transports (Ramezani and Nourinejad, 2018; Wei et al., 2020) among others.

Previous research corroborated that a pricing scheme can affect traveler behaviors, such as routing (e.g. Liu et al., 2013; Zheng and Geroliminis, 2020), mode choices (e.g. Basso and Jara-Díaz, 2012; Zheng et al., 2016), and departure times (e.g. Amirgholy and Gao, 2017; Kaddoura and Nagel, 2019). MFD-based congestion pricing schemes have been studied with the focus primarily limited to one or two urban regions. This paper pursues to introduce a pricing scheme based on MFD considering maintaining total generated toll revenue close to zero in a multi-region urban network to encourage public acceptance. To this end, we design a cordon congestion pricing method to obtain the optimal tolls of each region that concurrently minimizes the vehicles' total time spent and

* Corresponding author.
E-mail addresses: ye.li@sydney.edu.au (Y. Li), mohsen.ramezani@sydney.edu.au (M. Ramezani).

https://doi.org/10.1016/j.trc.2022.103932
Received 18 May 2022; Received in revised form 10 September 2022; Accepted 20 October 2022
Available online 15 November 2022

maintains quasi revenue-neutrality in the network by employing a bi-objective deep-learning-based model predictive control (MPC) approach.

1.2. Related works

MFD provides a low-scatter and concave relationship between mean weighted flow (or outflow) and vehicle accumulation (or density) of urban regions. Godfrey (1969) was the pioneer of this parsimonious modeling, while MFD idea was rejuvenated in Geroliminis and Daganzo (2008) with empirically observed data from Yokohama, Japan. The literature shows MFD of a heterogeneous network displays hysteresis loops (e.g. Gayah and Daganzo, 2011). Partitioning a heterogeneous urban network into several regions with uniform congestion distribution is an approach to obtain well-defined low-scatter MFDs (e.g. Saeedmanesh and Geroliminis, 2017; Saedi et al., 2020). The partitioning further enables introduction of region-based congestion pricing as an efficient traffic demand management approach for a large urban network that helps disperse vehicles to lessen vehicle accumulation in congested areas.

The MFD-based congestion pricing schemes have been proposed in several previous studies (e.g. Zheng et al., 2012; Simoni et al., 2015; Chen et al., 2016; Zheng et al., 2016; Dantsuji et al., 2019; Jakob and Menendez, 2021; Chen et al., 2021; Genser and Kouvelas, 2022). It is a common approach aiming to mitigate traffic congestion by imposing additional travel expenses to restrict excess demand from entering congested urban areas during rush hours. Several places have been successfully implemented congestion pricing schemes, e.g., ERP in Singapore, T-charge in London, OReGo in Oregon, and Congestion Tax in Gothenburg. Those achieved the goal of mitigating traffic congestion and relieving air pollution. A comprehensive review of congestion pricing practices can be found in Gu et al. (2018) and Lehe (2019).

Although most researchers (if not all) acknowledge that congestion pricing can economically and effectively alleviate traffic congestion, it faces many difficulties in implementation as well as public and political acceptance (Schuitema et al., 2010). One major fairness argument is that congestion pricing might end up taking more on low- and middle-income drivers than high-income drivers (Levinson, 2010) because these two groups are more likely to be priced off the road due to the lower value of time (Arnott et al., 1994). A trade-off exists between effectiveness and equity concerns that the congestion pricing would be less controversial if the revenues are spent to benefit low-income groups, such as supporting public transit or other travel incentives (Kristoffersson et al., 2017). Therefore, to encourage public acceptance, a congestion pricing scheme should consider softening the impact of economical and societal gaps. One solution is to design a quasi revenue-neutral tolling scheme, that is investigated in this paper.

The revenue-neutral concept implies all revenues that the government (road authority) gains from the pricing scheme are returned to the travelers (e.g. through public transport credits, tradable credit methods, or vehicle registration discount). For instance, a revenue-neutral pricing scheme may impose a direct positive toll on congested regions and a negative toll on uncongested regions, while preserving the aggregate total toll paid close to zero (Liu et al., 2009; Yang and Wang, 2011). Adler and Cetin (2001) created a mechanism wherein the revenue generated from commuters on the more desirable routes was directly paid to commuters driving on the less desirable routes. Nevertheless, network-level congestion pricing studies so far are mainly limited to diminish solely vehicles' total time spent. In light of this, this paper aims to propose a congestion pricing scheme that takes into account both improving network efficiency and persisting revenue-neutrality for multi-region networks. To find the optimal tolls to simultaneously achieve both objectives, the model predictive control (MPC) approach is utilized.

The MFD-based congestion management methods based on MPC, (e.g. Geroliminis et al., 2012; Ramezani et al., 2015; Csikós et al., 2017; Sirmatel and Geroliminis, 2021; Batista et al., 2021; Menelaou et al., 2021), primarily focus on perimeter flow control and regional routing. An MPC-based optimal congestion pricing has not been introduced for multi-region large urban networks on account of requiring excessive computational efforts. Network-level congestion pricing is studied using proportional–integral (PI) reactive control (e.g. Zheng et al., 2016; Gu and Saberi, 2021). To accomplish dual goals of improving network efficiency and keeping the tolling revenue-neutral, we propose a learning-based MPC method. A comparison between PI and MPC control strategies is investigated in Section 4.

The MPC framework consists of two models, i.e., prediction and simulation models.[1] The former is utilized to design the controller and the latter represents the plant (i.e., replicator of the real network). The MPC prediction model should be designed to require fewer and observable variables, feedback information, and traffic states. The proposed prediction model in this paper does not require the information of the destination of vehicles (a common modeling assumption in the literature). On the other hand, the MPC prediction model should consider the intricate route choice dynamics of vehicles, the effect of tolls on the route choice, and the transfer flows between the regions. To capture the complex dynamics of inter-region transfer flows and offer a precise estimation in the prediction model, we integrate a long-short term memory neural network (LSTM-NN) into the MPC framework. LSTM-NN is adopted owing to its adaptable model structure and learning capability, which has been used in disparate transport applications, such as traffic flow prediction (e.g. Jiang et al., 2014; Wu et al., 2018), and travel speed prediction (e.g. Ma et al., 2015; Gu et al., 2019). We integrate an LSTM-NN into the MPC framework to predict the proportions of inter-region transfer flows considering the impacts of regional demand, accumulation, as well as tolls; see more details in Section 2.2.

[1] The simulation model is not specific to the MPC framework and would be required for any computer simulation-based evaluation of feedback control methods.

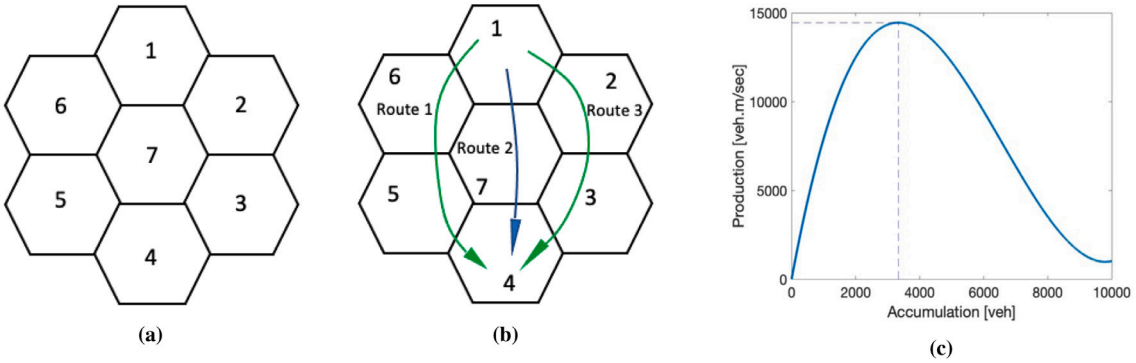

Fig. 1. (a) Network structure. A large-scale heterogeneous network comprising 7 homogeneous regions. Region 7 is the CBD of the network. (b) Three possible routes from Region 1 to Region 4. Green arrows show routes with less travel cost (greater travel distance but less toll) while the blue arrow represents the route with higher travel cost (shorter route, more congested route, more toll). (c) Well-defined MFD of each region. The dashed line indicates the critical accumulation with respect to the maximum production of MFD.

1.3. Contributions and paper structure

In this paper, the traffic flow dynamics of both prediction and simulation models are aggregated at the regional level, while the simulation model (plant) contains more details such as region to region origin–destination (OD) information, route choices, and boundary and receiving capacities. The network is divided into multiple regions, see Fig. 1, each is assumed to be homogeneously congested with a well-defined MFD (as shown in Fig. 1(c)). A simple en-route route choice model is integrated into the plant that takes k current lowest travel cost paths into account from the current region to the destination. Note that different numbers of shortest paths (i.e. k) are considered depending on the location of vehicles. Besides, the tolls in each region affect drivers' route choices since they tend to select the routes with lower travel costs (e.g. shorter distances or cheaper charges). Note that the route choice is realized in how the transfer flows between regions are modeled in the MPC prediction model.

Fig. 1(a) displays a schematic of the network that is split into seven homogeneous regions (shown as hexagons), and the centered region (i.e. Region 7) representing the CBD area which is expected to be more congested during morning peak hours because (i) it is the major destination of generated trips and (ii) it is the center of the network and on the shortest travel distance route between the majority of origins and destinations. Fig. 1(b) delineates three possible routes during the morning commute from Region 1 to Region 4, with the green arrows indicating less travel cost routes while the blue arrow illustrates a higher travel cost route since it passes CBD (because of higher toll and lower CBD speed). The congestion pricing strategy prevents the centered region from being overcrowded by incentivizing vehicles to switch routes, such that the vehicles are more uniformly distributed in the network. The proposed congestion pricing strategy is examined on a congested and heterogeneous network with directional travel demands. It should be mentioned that the proposed tolling scheme is primarily focused on altering travelers' route choice decisions in this paper, while mode choices and departure times are subject to further research. The proposed pricing is dynamic as the toll of each region fluctuates according to the current vehicle accumulations of the regions. Besides, the tolling scheme is cordon-based, that is travelers have to pay (or receive credit in case of negative toll) once they pass the regions boundaries. The total toll collected from a route is the sum of tolls for all passed regions except the origin and destination regions. This is a deliberate decision because travelers cannot freely shift their homes or working locations. Charging those people would lead to opposition to the pricing scheme implementation.

The principal contributions of this paper are threefold: (i) we develop a predictive congestion pricing scheme realized with a learning-based MPC controller to achieve dual objectives of improving network performance as well as maintaining the total toll revenue close to zero by crediting some drivers (negative tolls); (ii) the MPC pricing scheme is introduced and tested based on a multi-region network to investigate its effects on regional route choice of drivers; and (iii) an LSTM-NN is designed to estimate the percentage of inter-region transfer flows in the MPC prediction model. It should be mentioned that the majority of the studies (e.g. Mohajerpoor et al., 2020; Yildirimoglu et al., 2018; Sirmatel et al., 2021) assume (i) knowledge of vehicles' destinations and (ii) the ratio of inter-region outflows are instantaneously proportional to the destinations of vehicles. The proposed prediction model does not require the information of vehicles' destinations. Furthermore, integrating LSTM-NN relaxes assumption (ii) by learning the impacts of tolls on inter-region transfer flows from historical data.

The remainder of the paper is organized as follows. Section 2 presents the prediction model including the LSTM-NN utilized in the learning-based MPC framework. Section 3 introduces the optimal congestion pricing formulations employing the learning-based MPC as well as the simulation model applied to investigate the efficiency of the proposed pricing scheme. Section 4 illustrates the numerical results. The paper is summarized together with sketching future research directions in Section 5.

2. Prediction model

In this section, we develop a traffic flow model based on MFD to serve as the prediction model that the management approach (i.e., congestion pricing) is grounded on. The prediction model is developed without any destination region information to ease the

controller computational efforts, see Section 2.1. To accurately capture the interrelated dynamics of inter-region transfer flows and tolls in the prediction model, an LSTM-NN is integrated into the prediction model, see Section 2.2.

2.1. MFD traffic dynamics

We assume a large urban network is divided into R homogeneous regions, $\mathscr{R} = \{1, 2, \dots, R\}$. The proposed prediction MFD model describes the traffic dynamics of each region without requiring any region-to-region OD information. That is, there is no explicit consideration of the final destinations of vehicles and route choice in the prediction model so as to simplify the computational efforts of the controller. The prediction model tracks the movement of pockets of vehicles based on the regional transfer flows that are fundamentally a function of route choices and tolls. The relationship among inter-region transfer flows, tolls, and other traffic states is learned from historical data by the LSTM-NN. Note that the plant that is a more disaggregated model takes into account a detailed explicit current-best route choice model.

The prediction model formulates the evolution of vehicle accumulation in each region over time based on MFD dynamics. Each region demonstrates a well-defined MFD that relates the trip completion of the vehicles to the total number of vehicles inside the region. The trip completion rates can be estimated based on the MFD (e.g., a cubic-polynomial function of the number of vehicles in the region). Let $q_i(t)$ [veh/s] denote the exogenous traffic demand generated in Region i at time t, and $n_i(t)$ [veh] be the vehicle accumulation in Region i at time t; $i \in \mathscr{R}$. Therefore, the traffic flow conservation equation of the R-region prediction MFD model is,

$$\frac{\mathrm{d}n_i(t)}{\mathrm{d}t} = q_i(t) - g_i(n_i(t)) + \sum_{h \in \phi_i} m_h^i(t), \quad i \in \mathscr{R} \tag{1}$$

where ϕ_i is the set of regions that are closely connected with (are neighbors of) Region i. Note that $g_i(n_i(t))$ [veh/s] is the outflow MFD of Region i with accumulation of $n_i(t)$ at time t; $g_i(n_i(t)) = m_{ii}^i(t) + \sum_{h \in \phi_i} m_i^h(t)$. Here, $m_{ii}^i(t)$ [veh/s] is the internal trip completion rate of vehicles in Region i with final destination inside Region i (without passing another region), and $m_i^h(t)$ [veh/s] is the external outflow (inter-regional flow) of vehicles from Region i to the next immediate reachable Region h with any final destination regions inside the network. Accordingly, the external outflow is $m_i^h(t) = \sum_{j \in \mathscr{R}} m_{ij}^h(t)$, where $m_{ij}^h(t)$ [veh/s] is the external outflow from Region i with destination in Region j ($j \neq i$) through neighboring Region h at time t. It should be mentioned that the destinations of inter-region transfer flows are not considered in the prediction model while the model only requires the next immediate reachable regions. This is reasonable since the transfer flows must pass through one of the adjacent regions no matter where the destinations are (except that the region itself is the destination). Accordingly, the inter-region transfer flows can be estimated as,

$$m_i^h(t) = F_i^h(t) \cdot g_i(n_i(t)), \quad h \in \phi_i, \forall i \in \mathscr{R} \tag{2}$$

where $F_i^h(t)$ is the percentage of outflow from Region i to any destinations through adjoining Region h at time t. Evidently, $F_i^h(t)$ and $\Sigma_{h \in \phi_i} F_i^h(t)$ are between 0 and 1. Note that $F_i^h(t)$ is related to the route choice decisions of drivers and tolls as different regional tolls encourage and divert commuters from the overcrowded region to the less congested regions. The flow of transferring vehicles is typically approximated by the instantaneous ratio of vehicle accumulations based on their destinations. This assumption is abundant in literature (e.g. Liu and Geroliminis, 2017; Ingole et al., 2020; Batista et al., 2021) while it was relaxed in Li et al. (2021) for perimeter control design. Therefore, to describe and capture the nonlinear relationship of the aggregated regional dynamics an accurate estimation of inter-region transfer flows is necessary. We adopt an LSTM-NN to estimate $F_i^h(t)$. Introducing $F_i^h(t)$ simplifies the prediction model design thanks to the LSTM-NN that can replace the route choice models that require much more detailed information.

2.2. LSTM-NN for inter-region transfer flow estimation

In this section, an LSTM neural network is introduced to complement the prediction MFD model (i.e., Eq. (1)). LSTM neural network has been demonstrated its usefulness in transportation application (e.g. Cui et al., 2020; Roy et al., 2021; Sun and Kim, 2021). In this paper, the LSTM-NN is utilized to predict the percentage of transfer flows between regions, i.e. $F_i^h(t)$ in Eq. (2). Note that the predicted output of LSTM-NN is the portion of regional outflows, $F_i^h(t)$, instead of inter-region transfer flows, $m_i^h(t)$. This is a deliberate choice to improve the estimation accuracy since the outflow MFD can be directly obtained based on the number of vehicles.

We assume the percentage of outflows can be predicted grounded on regional accumulation, demand, and toll.[2] It should be noted that the regional accumulation contains the number of vehicles in the region itself and its surrounding regions, i.e. $n_i(t)$ and $n_h(t)$ where $h \in \phi_i$. Differently, only the tolls for the adjacent regions are considered, i.e. $\tau_h(t)$ denotes the toll of Region h ($h \in \phi_i$) at

[2] This paper assumes the speed MFD is a one-to-one (injective) function of accumulation. Accordingly, using accumulation data or speed data in theory should not change the accuracy of the LSTM-NN (trained) mapping with the current settings. Utilizing speed data is more applicable and sensible when simulation model is not based on the MFD.

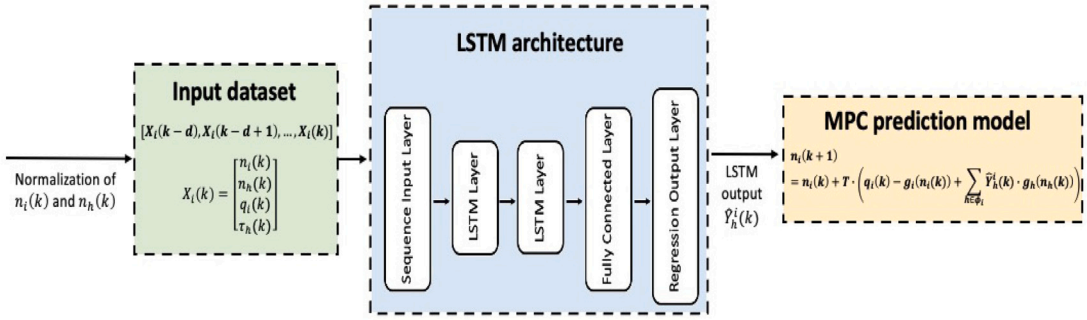

Fig. 2. LSTM neural networks architecture and integration with the MPC prediction model.

time t, since the toll value of the current region will not affect the next chosen region by the drivers. Accordingly, the time-dependent input vector of Region i, $X_i(t)$, for the LSTM-NN training and integration in the MFD dynamics, is defined as,

$$X_i(t) = \begin{bmatrix} n_i(t) \\ n_h(t) \\ q_i(t) \\ \tau_h(t) \end{bmatrix}, \quad h \in \phi_i. \tag{3}$$

The LSTM-NN estimates the percentage of outflows from Region i to any destinations through abutting Region h utilizing historical data, i.e. $\hat{Y}_i^h(t) = F_i^h(t)$,[3]

$$[\hat{Y}_i^h(t-d), \hat{Y}_i^h(t-d+1), \ldots, \hat{Y}_i^h(t)] = f(X_i(t-d), X_i(t-d+1), \ldots, X_i(t)), \tag{4}$$

where f represents the functional form of the trained LSTM-NN, X_i are values of network state vector, and d is positive varying time lags set to train the LSTM-NN. The LSTM-NN output, $\hat{Y}_i^h(t)$, is the estimated percentage of outflows from Region i through neighboring Region h. The outputs in Eq. (4) are all percentage of outflows corresponding to the inputs of previous time steps while only the last one (at current time t) is applied in Eq. (1). Note that the number of LSTM-NN outputs (i.e. percentage of transfer outflows) for Region i is identical to the number of its neighbor regions. For example, Region 7 LSTM-NN has 6 outputs at each time step, [4] which are $\hat{Y}_7^1, \hat{Y}_7^2, \hat{Y}_7^3, \hat{Y}_7^4, \hat{Y}_7^5$, and $\hat{Y}_7^6$. Similar to $F_i^h(t)$, the value of $\hat{Y}_i^h(t)$ and $\Sigma_{h \in \phi_i} \hat{Y}_i^h(t)$ are between 0 and 1. The LSTM-NNs are trained using historical data until convergence achieved. Details of configuration, training, and validation of the LSTM-NN are presented in Appendix.

The percentage of inter-region outflows dataset employed to train the LSTM-NN are generated from the simulation model considering randomness in demands, tolls, etc., so as to enhance the predictability of the LSTM-NN. Note that these training data can readily be substituted with field data. Therefore, the inter-region transfer flows in Eqs. (1) and (2) can be written as,[5]

$$m_i^h(t) = F_i^h(t) \cdot g_i(n_i(t)) = \hat{Y}_i^h(t) \cdot g_i(n_i(t)) \quad \forall i \in \mathscr{R}, h \in \phi_i. \tag{5}$$

Ultimately, the trained LSTM-NNs are applied to estimate the percentage of inter-region transfer flows in the prediction model of the MPC, as sketched in Fig. 2.

3. Model predictive control

In this section, the learning-based MPC controller is introduced to determine the time-varying toll of each region utilizing the prediction model that integrates MFD modeling and LSTM-NN predictions. To improve network performance and maintain revenue-neutrality, MPC is an effective approach to combine and accomplish the bi-objective optimization. The overall learning-based MPC architecture for the proposed congestion pricing strategy is depicted in Fig. 3.

Model predictive control framework consists of two models, the prediction model and the simulation model. Both prediction and simulation models are based on MFD dynamics but at different levels of aggregation. The prediction model, which is employed to obtain the optimal tolls of each region, is grounded on regional states, i.e., region accumulation n_i, without the requirement of knowing the destination information. The LSTM-NN is embedded in the prediction model to estimate the percentage of inter-region transfer flows by accounting for the impacts of regional tolls on the route choices. Note that the prediction model requires

[3] The sequence-to-sequence LSTM-NN is employed to predict the percentage of outflows such that several outputs correspond to past values. We tested sequence-to-one LSTM-NN, with only one output $\hat{Y}_i^h(t)$, and the obtained performance was worse than sequence-to-sequence LSTM-NN.

[4] We separately train the LSTM-NN for each region instead of training only one LSTM-NN for the whole network in order to improve accuracy.

[5] The MFD model integrated with LSTM-NN in Eq. (1) and (5), satisfies the network-level mass conservation rule irrespective of the accuracy of LSTM-NNs. However, the regional distribution of accumulations might exhibits discrepancies with respect to OD demand pairs. Nevertheless, the recurrent feedback structure of MPC diminishes the modeling error accumulation over time.

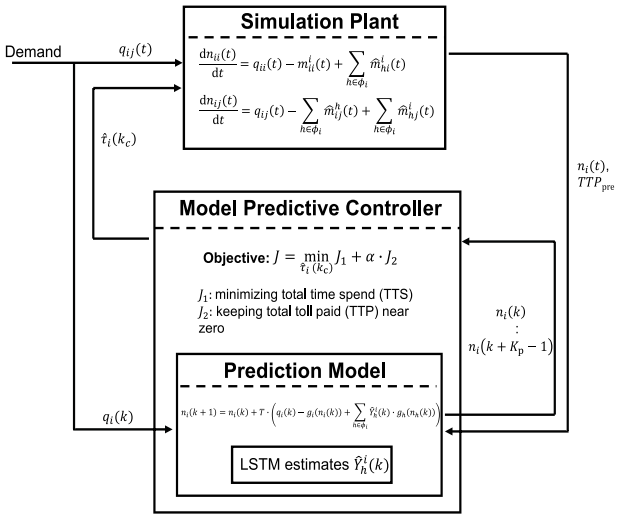

Fig. 3. The control architecture of the proposed congestion pricing management approach based on MPC. The aggregated prediction MFD model including the LSTM-NN predictor for the percentage of inter-region transfer flows is employed to design the controller. The detailed MFD model (simulation plant) is considered to represent real multi-region traffic network.

information (e.g., regional accumulation, total toll paid by vehicles in previous times) provided by the simulation model (plant). The simulation model tracks the traffic flow dynamics in detail from the origin region to the destination region, which requires considering route choices between origin and destination regions and the constraints on the inter-region transfer flow by the receiving and boundary capacities. Details of the simulation model are discussed in Section 3.1.

3.1. Simulation model

In this section, a detailed MFD model is introduced to depict the plant (i.e. real network) dynamics of a multi-region network. This model describes detailed aggregated traffic dynamics of each region, integrates a current-best route choice model considering the travel cost of possible routes between each OD pair (i.e. every two regions), and contains the effect of the boundary and receiving capacities (see subregion-based model of Ramezani et al. (2015) and Li et al. (2021)). Note that the number of routes between each regional OD pair is not fixed, meaning that the route choice model considers a few numbers of current-best paths for close regions and more paths if the origin and destination regions are far from each other.

Let $n_{ij}(t)$ [veh], $i, j \in \mathcal{R}$, denote the accumulation of vehicles in Region i with final destination in Region j at time t. Intuitively $n_i(t) = \sum_{j=1}^{R} n_{ij}(t)$ [veh], where R is the total number of regions in the network. The (internal) trip completion of vehicles in Region i at time t is denoted by $m^i_{ii}(t)$ [veh/s], and the external outflow of vehicles in Region i with final destination Region j through the immediate reachable Region h is denoted by $m^h_{ij}(t)$ [veh/s], $h \in \phi_i$. Assuming the outflows ratio is proportional to destinations of vehicles, the internal and external outflows of Region i are,

$$m^i_{ii}(t) = \frac{n_{ii}(t)}{n_i(t)} \cdot \frac{p_i(n_i(t))}{l_{ii}(t)} \tag{6a}$$

$$m^h_{ij}(t) = \theta^h_{ij}(t) \cdot \frac{n_{ij}(t)}{n_i(t)} \cdot \frac{p_i(n_i(t))}{l_{ih}(t)}, \quad i \neq j, h \in \phi_i, \tag{6b}$$

where $p_i(n_i(t))$ [veh m/s] is the production MFD of homogeneous Region i; and $l_{ii}(t)$ and $l_{ih}(t)$ [m] are the vehicles' average trip length inside Region i and traveling from Region i to Region $h \in \phi_i$.

The detailed simulation model integrates a simple regional route choice model, where $\theta^h_{ij}(t)$ is estimated using a logit model based on the travel cost from Region i to j through the current-best (less travel cost) paths (i.e. a series of regions). Note that $\theta^h_{ij}(t) \in [0, 1]$ shows the time-varying proportion of vehicles in Region i with final destination in Region j that the immediate reachable region in their path is Region h. Evidently, we have $\sum_{h\in\phi_i} \theta^h_{ij}(t) = 1$. It should be mentioned that the instantaneous travel cost of each route between any two regions is determined by summing the instantaneous trip travel time (through the regions on the route) and tolls of all passing regions except the current and destination regions.[6] For example, in Fig. 1(b), the total travel cost at time t from Region 1 to Region 4 through a possible route, e.g. Route 1 (i.e. the sequence of regions, 1-6-5-4) is $TC^{\text{Route1}}_{14}(t) = tc_1(t) + tc_6(t) + tc_5(t) + tc_4(t)$, where $tc_i(t)$ is the travel cost of Region i at time t which is determined based on the value of time of travelers and travel time in

[6] Certainly, tolls can force travelers choose other departure time or traffic modes, while merely route choice behavior is considered in this paper to understand how travelers avoid paying travel fees.

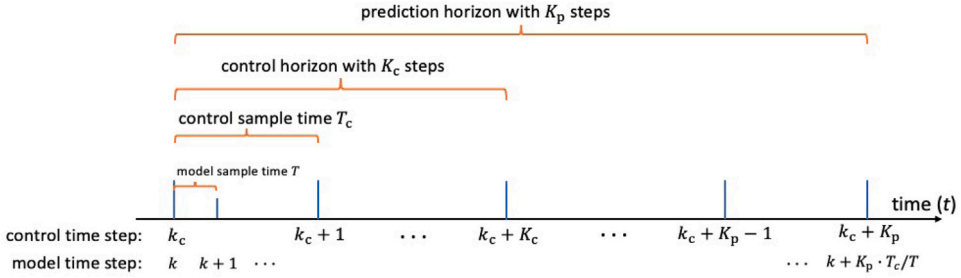

Fig. 4. Relationship between different time intervals and time steps of MPC formulation.

Region i. Note that the travel cost is in monetary unit. We assume all travelers have the same value of time (VOT [monetary unit/s]). Thus, $tc_i(t) = \text{VOT} \cdot tt_i(t) + \tau_i(t)$, where $tt_i(t)$ [s] and $\tau_i(t)$ [monetary unit] are respectively the expected travel time and the toll of Region i at time t. Remind that, we assume no tolls collected from the origin and destination regions, therefore the total travel cost of Route 1 is $TC_{14}^{\text{Route1}}(t) = tt_1(t) \cdot \text{VOT} + tt_6(t) \cdot \text{VOT} + \tau_6(t) + tt_5(t) \cdot \text{VOT} + \tau_5(t) + tt_4(t) \cdot \text{VOT}$. Note that the expected travel time in Region i at time t, $tt_i(t)$, can be estimated as the ratio of the average travel distance inside Region i divided by the region average speed $v_i(t)$ [m/s]. The speed of Region i at time t can be estimated from the region MFD, i.e. $v_i(t) = p_i(n_i(t))/n_i(t)$.

The simulation model also integrates the effects of boundary and receiving capacities to realize if the neighboring Region h has enough space to accommodate incoming transfer flows. Accordingly, the realized outflow from Region i heading to destination Region j through Region h, $\hat{m}_{ij}^h(t)$ [veh/s], is estimated from the minimum of the outgoing transfer flow ($m_{ij}^h(t)$), boundary capacity between Region i and h (b_{ih} [veh/s]), and a part of receiving capacity of Region h ($r_h(n_h(t))$ proportional to the incoming transfer flows from all regions around Region h (for more details refer to Li et al. (2021)):

$$\hat{m}_{ij}^h(t) = \min\left(m_{ij}^h(t), b_{ih}, \frac{m_{ij}^h(t)}{\sum_{s\in\phi_h}\sum_{e\in\mathscr{R},s\neq e} m_{se}^h(t)} \cdot r_h(n_h(t)) \right). \tag{7}$$

The receiving capacity of Region h, $r_h(n_h(t))$ [veh/s], is determined by $r_h(n_h(t)) = r_h^{\max} \cdot (1 - n_h(t)/n_h^{\text{jam}})$, where $r_h^{\max}$ [veh/s] is the maximum receiving capacity of Region h, and n_h^{jam} [veh] is the jam accumulation of Region h. The estimation of the definite form of regional receiving capacity need further investigations and validation with field data.

Let $q_{ij}(t)$ [veh/s] be the exogenous traffic demand generated in Region i with final destination Region j, so we have $q_i(t) = \sum_{j=1}^{R} q_{ij}(t)$ [veh/s]. Ultimately, the traffic dynamics of the simulation model are ($i, j \in \mathscr{R}$):

$$\frac{\mathrm{d}n_{ii}(t)}{\mathrm{d}t} = q_{ii}(t) - m_{ii}^i(t) + \sum_{h\in\phi_i} \hat{m}_{hi}^i(t), \tag{8a}$$

$$\frac{\mathrm{d}n_{ij}(t)}{\mathrm{d}t} = q_{ij}(t) - \sum_{h\in\phi_i} \hat{m}_{ij}^h(t) + \sum_{h\in\phi_i} \hat{m}_{hj}^i(t) \quad i \neq j. \tag{8b}$$

Note that the simulation model tracks the vehicle accumulations with respect to their destinations while this is not considered in the prediction model to reduce the MPC computation cost and to relax the need for destination estimation to ease the field implementation. That is, the simulation model of the 7-region network requires 49 states ($n_{ij}(t)$), whereas the number of traffic states in the prediction model is 7 $n_i(t)$.

3.2. The MPC formulation

The MPC controller uses the dynamic prediction model (containing the LSTM-NN) to predict the future evolution of traffic states and select the optimal control action (i.e. time-varying toll of each region) in a receding horizon manner. In the MPC framework, there are different time intervals and steps associated with the design and implementation of MPC with respect to the model and control updates. That is, the model (discrete) interval indicates how often the model predicts traffic dynamics (i.e. regional accumulations), and the control interval denotes how often the control actions (i.e. tolls of each region) change. As illustrated in Fig. 4, the objective function is optimized at each control time step (e.g. each time step with a duration of 600 [s]) over a prediction horizon of K_p, assuming a control horizon of K_c possible changes in the control actions, with $K_c \leq K_p$. The first optimal control sequence is then applied to the plant (i.e. applying the optimal toll of each region for 600 [s] and discarding the remaining samples). Let k_c [-] and T_c [s] be the control time step and the control sample time, respectively. Note that the discrete (model) time step and time step duration of the prediction model, k [-] and T [s], are different from the duration of the control time step and control sample time. The reason is that MPC is activated only when a control time step is fully elapsed.

The associated MPC optimization problem is formulated as:

$$J_1 = \min_{\hat{\tau}_i(k_c)} T \cdot \sum_{k=k_c}^{k_c+K_p\cdot T_c/T} \sum_{i\in\mathscr{R}} n_i(k) \tag{9a}$$

$$J_2 = \min_{\hat{\tau}_i(k_c)} \left(T \cdot \sum_{k=k_c}^{k_c+K_p \cdot T_c/T} \sum_{i \in \mathscr{R}} \sum_{h \in \phi_i} \hat{Y}_i^h(k) \cdot g_i(n_i(k)) \cdot \tau_h(k) + TTP_{\text{pre}} \right)^2 \tag{9b}$$

subject to

$$X_i(k) = [n_i(k), n_h(k), q_i(k), \tau_h(k)]^\top, \quad h \in \phi_i \tag{9c}$$

$$[\hat{Y}_i^h(k-d), \hat{Y}_i^h(k-d+1), \dots, \hat{Y}_i^h(k)] = f(X_i(k-d), X_i(k-d+1), \dots, X_i(k)) \tag{9d}$$

$$n_i(k+1) = n_i(k) + T \cdot \left(q_i(k) - g_i(n_i(k)) + \sum_{h \in \phi_i} \hat{Y}_h^i(k) \cdot g_h(n_h(k)) \right), \quad \forall i \in \mathscr{R} \tag{9e}$$

$$0 \le n_i(k) \le n_i^{\text{jam}}, \quad \forall i \in \mathscr{R} \tag{9f}$$

$$0 \le \hat{Y}_i^h(k) \le 1, \quad \forall i \in \mathscr{R}, h \in \phi_i \tag{9g}$$

$$0 \le \sum_{h \in \phi_i} \hat{Y}_i^h(k) \le 1, \quad \forall i \in \mathscr{R} \tag{9h}$$

$$\tau_i^{\min} \le \hat{\tau}_i(k_c) \le \tau_i^{\max}, \quad \forall i \in \mathscr{R}. \tag{9i}$$

where J_1 and J_2 represent the objective functions indicating the vehicles total time spent in the network and square of the total toll collected from the travelers. The first term of the right hand side of J_2, denotes the generated tolls (possibly negative) in the current control time duration. Moreover, there is another source of approximation in J_2, i.e. $\sum_{k=k_c}^{k_c+K_p \cdot T_c/T} \sum_{i \in \mathscr{R}} \sum_{h \in \phi_i} \hat{Y}_i^h(k) \cdot g_i(n_i(k)) \cdot \tau_h(k)$, in which $\hat{Y}_i^h(k)$ is used as the actual transfer flow ratios. It implies that the total toll paid is not necessarily equal to 0 even if MPC attains $J_2 = 0$ and applies the optimal tolls to the plant. n_i^{jam} [veh] is the jam accumulation of Region i, and $\tau_i^{\min}$ and $\tau_i^{\max}$ are respectively the prescribed lower and upper bounds of Region i's toll. The regional toll constraints within the bounds are to refrain overcharging as well as keeping the total toll revenue neutral (because $\tau_i^{\min}$ allows negative values). Besides, TTP_{pre} is the total toll paid (by all drivers) from time zero up to the current time. The optimization problem (i.e. Eq. (9)) is a nonlinear optimization problem that can be solved numerically by nonlinear optimization algorithms. The optimization variables over control horizon are $\hat{\tau}_i(k_c) = [\tau_i(k_c), \dots, \tau_i(k_c + K_c - 1)]^\top$, where $\tau_i(k_c + l)$ for $l = 0, \dots, K_c - 1; i \in \mathscr{R}$ are the optimized tolls by MPC pricing controller. Eqs. (9c) and (9d) denote the use of trained LSTM-NN to estimate the percentage of inter-region transfer flows. In Eq. (9d), the functional handle f represents the trained sequence-to-sequence LSTM-NN, and only the last estimated percentage of inter-region transfer flow (i.e. $\hat{Y}_i^h(k)$) will be utilized in calculating network dynamics. Particularly, d is the positive time lag utilized in LSTM-NN training procedure. When calling LSTM-NN, the input data requires to be consistent with the time step used during training. Note that Eq. (9e) is the discrete version of the network dynamics (i.e. Eq. (1)). Also note that $\hat{Y}_h^i(k)$ is predicted by the pre-trained LSTM neural networks, and the nonlinear constraints, i.e. Eq. (9g) and (9h), are set to ensure the LSTM-assisted MFD model satisfies the conservation law of regional flows.

It is worth mentioning that the goals of the proposed congestion pricing scheme are minimizing vehicles' total time spent while preserving total toll paid near zero (i.e. revenue-neutrality) by adopting MPC to simultaneously minimizes both objectives. Therefore we combine the two objectives (i.e. Eq. (9a) and (9b)) as one,

$$J = \min_{\hat{\tau}_i(k_c)} J_1 + \alpha \cdot J_2, \tag{10}$$

where α is the weighting parameter regulating the relative importance of the two parts of the overall MPC objective function J.

4. Numerical experiments

In this section, we present the results of simulation experiments to explore the performance of the proposed congestion pricing scheme on the multi-region network. In subsequent sections, we first describe the settings of the experiments and then present the result of the studied scenarios.

4.1. Simulation settings

The studied network consists of seven regions with Region 7 as the city center, schematically shown in Fig. 1(a). We presume all regions with identical MFD (without loss of generality) consistent with the one observed in Yokohama (see Geroliminis and Daganzo, 2008), where $p_i(n_i(t)) = 3.4216 \cdot 10^{-4} \cdot n_i(t)^3 - 6.8575 \cdot n_i(t)^2 + 3.4710 \cdot 10^4 \cdot n_i(t)$, $\forall i \in \mathscr{R}$, see Fig. 1(c). Correspondingly, the critical accumulation that maximizes the regional outflow is $n_i^{\text{cr}} = 3392$ [veh], and the jam accumulation is $n_i^{\text{jam}} = 10000$ [veh]. A typical time-varying peak period travel demand is considered for 3600 [s], followed by another 3600 [s] period with negligible demand to ensure the network is completely cleared at the end of simulation. The network is initially in uncongested condition for all regions, with regional accumulation of $n_1(0) = 3003, n_2(0) = 1613, n_3(0) = 2084, n_4(0) = 1946, n_5(0) = 2774, n_6(0) = 1711$, and $n_7(0) = 1368$ [veh].

The number of shortest paths between regions is determined by the vehicle's current location in the network. The contiguous regions have relatively few numbers of current-best route choices, e.g. the number of shortest paths is 2 if neither origin nor destination is Region 7 while 3 if either region is Region 7. On the contrary, 7 shortest paths are considered as the choice set of the current-best route choice procedure for the nonadjacent regions.

Table 1
Network-level statistics (averaged over 10 replications) for the studied scenarios. The numbers in parenthesis indicate the improvement in performance compared with the No toll scenario. The total number of vehicles is 66064 [veh]. Note that "$\tau^{\min} < 0$" means the minimum toll in related scenario is negative (i.e. $\tau^{\min} = -\text{fftt} \cdot \text{VOT}$). The results of sensitivity analysis on α are included.

Pricing scenario	Total time spent [veh h]	Average travel time [min/veh]	Total toll paid [$]	Average toll paid [$/veh]
No toll	3.19×10^4	29.0	0	0
PI ($\tau^{\min} = 0$)	2.90×10^4 (−9.12%)	26.3	93404	1.41
PI ($\tau^{\min} < 0$)	2.84×10^4 (−10.91%)	25.8	75948	1.15
MPC ($\tau^{\min} = 0$, $\alpha = 0$)	2.89×10^4 (−9.45%)	26.2	92482	1.40
MPC ($\tau^{\min} < 0$, $\alpha = 0$)	2.83×10^4 (−11.25%)	25.7	69990	1.01
MPC ($\tau^{\min} < 0$, $\alpha = 0.1$)	3.05×10^4 (−4.4%)	27.7	26764	0.41
MPC ($\tau^{\min} < 0$, $\alpha = 0.5$)	2.82×10^4 (−11.66%)	25.6	6158	0.09
MPC ($\tau^{\min} < 0$, $\alpha = 2$)	2.95×10^4 (−7.52%)	26.8	−86	−0.001
MPC ($\tau^{\min} < 0$, $\alpha = 10$)	2.94×10^4 (−7.84%)	26.7	−3457	−0.05

The toll values of each region are determined through the proposed learning-based MPC. The selected MPC parameters are: the control horizon $K_c = 2$ and the prediction horizon $K_p = 6$. The objective function weighting parameter $\alpha = 0.5$ if considering revenue-neutral goal, otherwise $\alpha = 0$. The toll values are constrained between the lower bound $\tau_i^{\min} = 0$ and the upper bound $\tau_i^{\max} = 5$ in USD. It should be mentioned that the lower bound becomes negative when considering crediting drivers, in which case the lower bound is determined through regional free-flow travel time (fftt). That is $\tau_i^{\min} = -\text{fftt}_i \cdot \text{VOT}$, where the VOT is the predefined average value of time, selected equal to 16 [USD/hr]. Note that all commuters are assumed to have the same VOT. To consider heterogeneous VOT for travelers, a possible future research direction is to use the trip-based MFD model that considers each traveler's detailed travel characteristics (see Mariotte et al., 2017; Li et al., 2021) instead of accumulation-based MFD model as the simulation plant.

Besides, a proportional–integral (PI) controller is adopted for comparison purposes. The PI control is implemented as a model-free reactive controller that can iteratively modify the tolls based on the difference between current accumulation and the desired accumulation. We set $n_i^{\text{desired}} = 95\% \cdot n_i^{\text{cr}}$ as the desired accumulation. Correspondingly, the toll of Region i is adjusted via the PI controller described by $\tau_i(k_r) = \tau_i(k_r - 1) + I_p \cdot (n_i(k_r) - n_i(k_r - 1)) + I_i \cdot (n_i(k_r) - n_i^{\text{desired}})$, where proportional and integral gains are respectively chosen as $I_p = 0.003$ and $I_i = 0.001$, and k_r is the toll updating time step with $k_r = 1, 2, \ldots$. Considering the fact that updating regional tolls within short intervals is not realistic from an operation perspective, both controllers (i.e. PI and MPC) amend the tolls every 10 min (i.e. 600 [s]). Note that a turn-off policy for either control approach is utilized, which applies zero toll in each region if all regional accumulations are less than a certain value (i.e. the critical accumulation).

4.2. Results and discussion

We compare six control scenarios to scrutinize the performance of the proposed congestion pricing scheme: (i) No toll where applied tolls are zero for all regions over the whole simulation period, (ii) PI control with the minimum toll in each region equals to zero ($\tau^{\min} = 0$), (iii) PI control with negative minimum toll in each region where negative toll is determined by free-flow travel time times average VOT ($\tau^{\min} = -\text{fftt} \cdot \text{VOT}$), (iv) MPC with minimum toll in each region and the objective function weighting parameter equal to zero ($\tau^{\min} = 0$, $\alpha = 0$), (v) MPC with negative minimum toll in each region and the objective function weighting parameter equal to zero ($\tau^{\min} = -\text{fftt} \cdot \text{VOT}$, $\alpha = 0$), and (vi) MPC with negative minimum toll in each region and non-zero objective function weighting parameter ($\tau^{\min} = -\text{fftt} \cdot \text{VOT}$, $\alpha = 0.5$). Note that the upper bound of tolls in each region is 5 USD for all scenarios (i.e. $\tau^{\max} = 5$). These experiments enable us to highlight the efficiency and revenue-neutrality of the proposed congestion pricing method.

Fig. 5(a) depicts the evolution of regional accumulations over the studied period for the No toll scenario. With the absence of tolls, the toll values always operate at zero such that several regions, i.e. Regions 1, 3, 4, and 5, become congested while Region 7 (CBD) becomes heavily congested. Regions 2 and 6 remain uncongested all along the studied period while their extra capacity to accommodate vehicles can be realized with a well-designed pricing scheme. Besides, it can be observed that the accumulation difference among the regions is considerable, i.e. the maximum accumulation is 7823 [veh] in Region 7 and 2996 [veh] in Region 2. In the No toll scenario, the average travel time per vehicle is 29 [min], see Table 1 where the vehicles' total time spent (TTS) in the network [veh h], average travel time [min/veh], the total toll paid (TTP) [$], and average toll paid [$/veh] in the network as a result of implementing the various pricing strategies are listed. The reported results are obtained through the average outcomes of ten replications. The numbers inside parentheses corresponding to TTS are the change in the percentage of total network performance compared with the No toll scenario.

The results of implementing (PI and MPC) controllers are exhibited in Fig. 5(b)–(f) and Fig. 6 where the time-varying regional accumulations $n_i(t)$ and tolls $\tau_i(t)$ over the studied period are delineated. It is obvious that applying both controllers, i.e. PI and MPC, lead to clearing the network earlier than the No toll scenario. When applying PI control with zero minimum toll ($\tau^{\min} = 0$), as shown in Fig. 5(b), the accumulation is more homogeneously distributed compared to the No toll scenario (Fig. 5(a)); the maximum accumulation difference is 2745 [veh] (4227 [veh] for the No toll case). The accumulation in Region 7 is diverted to other regions such that more vehicles are traveling through Regions 2, 3, 5, and 6. The reason is that the drivers tend to choose the routes with less travel cost whereas the toll in Region 7 grows rapidly and reaches the maximum value (i.e. $\tau^{\max}$) and remains at the maximum

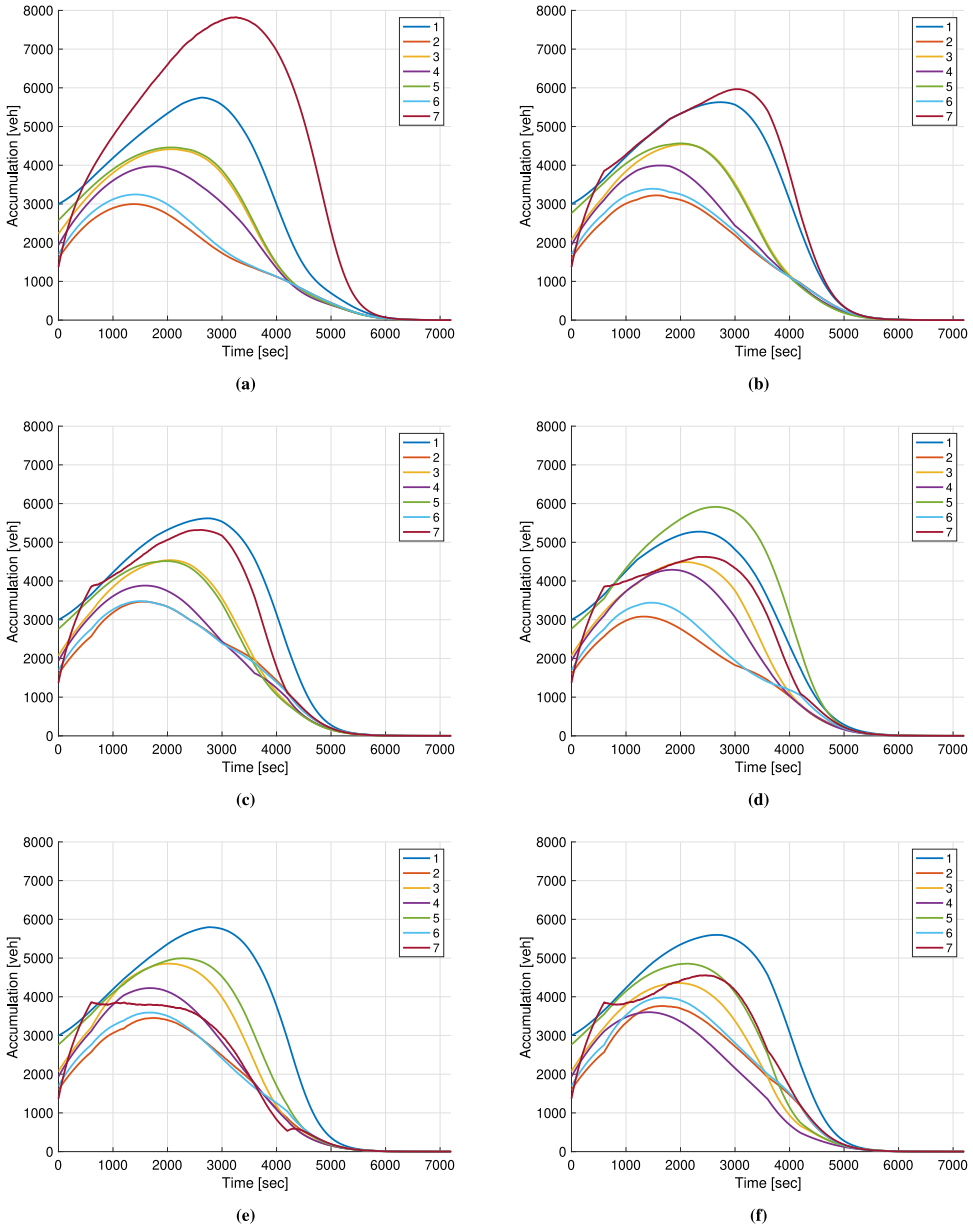

Fig. 5. Regional accumulation evolution for the whole studied period obtained from simulations when applying the following pricing strategies: (a) No toll; (b) PI with $\tau^{\min} = 0$; (c) PI with $\tau^{\min} = -\text{fftt} \cdot \text{VOT}$; (d) MPC with $\tau^{\min} = 0$ and $\alpha = 0$; (e) MPC with $\tau^{\min} = -\text{fftt} \cdot \text{VOT}$ and $\alpha = 0$; (f) MPC with $\tau^{\min} = -\text{fftt} \cdot \text{VOT}$ and $\alpha = 0.5$. In the No toll scenario, several regions (i.e. Regions 1, 3, 4, 5, 7) become congested, while Regions 2 and 6 are uncongested. Utilizing MPC revenue-neutral pricing method contributes to a more homogeneous accumulation distribution in the whole network as well as shorter network clearance time compared to the PI control.

value for a long period (from 2400 to 4200 [s]), as portrayed in Fig. 6(a). In this scenario, the total time spent (TTS) of vehicles in the whole network is 9.12% less compared with the No toll scenario, see Table 1. The average travel time and average toll imposed on a vehicle are 26.3 [min] and $1.41, respectively.

The results of scenario (iii) demonstrate allowing negative minimum tolls improves the performance of the PI control strategy to recover the network from the protracted congestion experienced in Region 7 where the congested period reduced from 3600 [s] to 3100 [s], as shown in Fig. 5(c). Besides, the accumulation heterogeneity of the network is further mitigated with PI with negative tolls such that the maximum accumulation difference is 2153 [veh] between Regions 1 and 2. This shows crediting travelers can encourage them to switch routes, and subsequently, the vehicles are detoured to avoid congested regions with higher tolls to reduce their travel costs. As displayed in Table 1, the TTS of PI control with negative tolls is 10.91% less than the No toll scenario. The negative tolls reduce average toll paid by a vehicle; 18.5% reduction compared to PI with $\tau^{\min} = 0$.

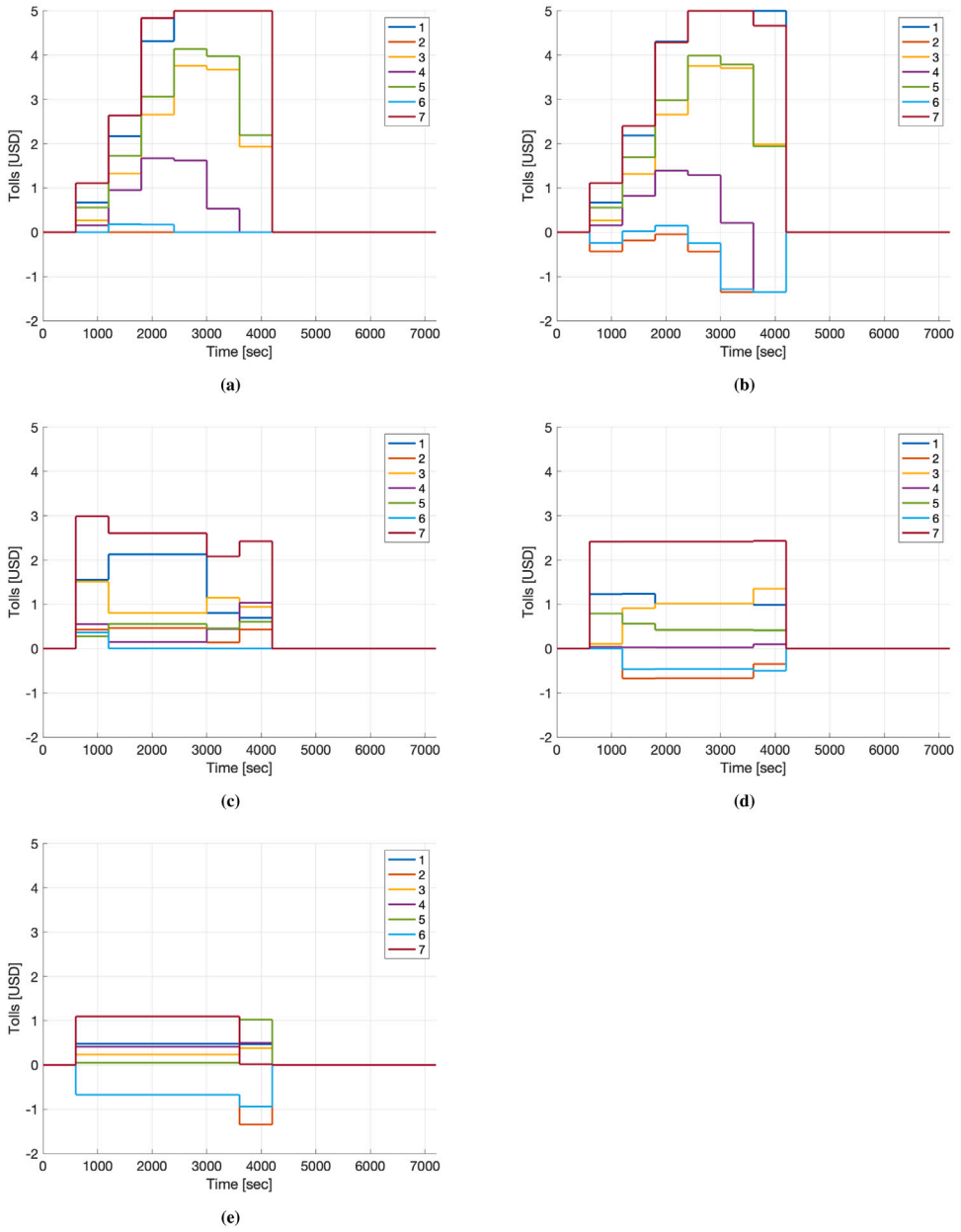

Fig. 6. Toll in each region during the simulation period when applying the following pricing strategies: (a) PI with $\tau^{\min} = 0$; (b) PI with $\tau^{\min} = -\mathrm{fftt} \cdot \mathrm{VOT}$; (c) MPC with $\tau^{\min} = 0$ and $\alpha = 0$; (d) MPC with $\tau^{\min} = -\mathrm{fftt} \cdot \mathrm{VOT}$ and $\alpha = 0$; (e) MPC with $\tau^{\min} = -\mathrm{fftt} \cdot \mathrm{VOT}$ and $\alpha = 0.5$. For all scenarios, $\tau^{\max} = 5$. The average toll paid per vehicle for the five scenarios are \$1.41, \$1.15, \$1.40, \$1.01, and \$0.09, respectively.

MPC control strategies considering single objective of minimizing TTS (Fig. 5(d)–(e), $\alpha = 0$) outperform the PI controller (Fig. 5(b)–(c)) in both scenarios with $\tau^{\min} = 0$ and $\tau^{\min} < 0$, in a way that the PI controller leads to congestion of Region 1 and Region 7 for a longer period, resulting in additional delay. It can be observed in MPC control scenarios that Region 7 is less crowded with curtailed congestion. A similar trend with PI control can be found with MPC that the network accumulation is more evenly distributed across regions. MPC with negative minimum toll (Fig. 5(e)) is successful in uniformly dispersing vehicles in the whole network compared to MPC with zero minimum toll (Fig. 5(d)), such that the maximum accumulation difference reduces from 2834 [veh] to 2345 [veh]. Note that crediting drivers can promote them to adjust routes by using less congested regions. This is identified in Fig. 5(e) and Fig. 6(d), as the accumulations in Regions 2 and 6 are respectively increased when the corresponding tolls are more favorable (negative tolls), see the jumps in vehicle accumulations of Region 2 and Region 6 at 1200 [s], and their corresponding higher accumulation till 4200 [s] (compared to Fig. 5(d)). Moreover, the MPC control strategy is effective in decreasing vehicles' TTS, in the $\tau^{\min} = 0$ scenario, 9.45% reduction compared to the No toll scenario. While considering negative tolls in MPC not only

helps reduce TTS by 11.25% compared to the No toll scenario, the average toll paid per vehicle is approximately 24.32% less than MPC with zero minimum toll, see Table 1. Results indicate that allowing negative tolls can improve public acceptability of the pricing scheme by decreasing both the drivers' travel time and paid tolls.

Furthermore, the quasi revenue-neutral MPC controller ($\tau^{\min} < 0$, $\alpha = 0.5$) accomplishes to keep the network in better states even at a lower generated toll. As displayed in the time series of tolls for all regions in Fig. 6(e), the toll in Regions 2 and 6 remain at smaller negative values for a longer period, while other regions charge relatively lower tolls (not more than \$1.2). It is illustrated in Table 1 that the MPC controller considering revenue-neutrality ($\alpha = 0.5$) minimizes the combined objective (i.e. Eq. (10)), in a way that it dwindles the TTS by approximately 11.66% with respect to the No toll scenario as well as drops the TTP closer to zero compare against PI and MPC with $\alpha = 0$ scenarios. Besides, to evaluate the relative weight of the revenue neutrality measure in the objective function, the results of sensitivity analysis with various α are displayed in Table 1. It can be observed that $\alpha = 0.5$ outperforms other scenarios (i.e. $\alpha = 0.1$, 2, and 10) with respect to TTS. In terms of TTP, to a great degree, increasing α would result in lower total toll paid (TTP) values. Noteworthy, $\alpha = 2$ and 10 lead to negative TTP values. A notable point to consider is that the effect of α is not straightforward in obtaining the Pareto front of TTS and TTP. The reason is that α controls the trade off between J_1 and J_2 in the objective function of MPC, see Eq. (10); while J_1 is TTS, J_2 is an approximation of TTP and thus fine-tuning α might exhibit minor unexpected fluctuations in TTP values.

The applied toll in each region obtained from the PI and MPC pricing scenarios are portrayed in Fig. 6. At very beginning of the simulation time (from 0 to 600 [s]), there is no toll since all regions are uncongested. Afterward, as Regions 1 and 7 become congested, the controllers pursue to protect these two regions by implementing relative greater toll values, since without any restriction Region 7 will become hyper congested, see the regional accumulation evolution for the No toll scenario in Fig. 5(a). In addition, the toll values with PI control (Fig. 6(a), (b)) frequently fluctuate compared against the MPC control scenarios (Fig. 6(c), (d)), particularly, between $t = 600$ [s] and $t = 4200$ [s], which is the most congested duration. The toll values with PI control in either scenario cover the overall range of the toll spectrum (i.e. between $\tau^{\min}$ and $\tau^{\max}$). On the contrary, the actual toll values of MPC control scenarios (Fig. 6(c), (d), (e)) show a relatively limited range, not reaching to the toll bounds.

5. Summary and future research

This paper has studied a network-level congestion pricing strategy based on the MPC approach to address dual objectives of improving network performance as well as maintaining the toll revenue neutral (by crediting some travelers). Two different aggregation level models are derived based on the MFD dynamics, i.e. the prediction model of the MPC framework is modeled in an aggregated manner using regional accumulations (without destination information) while the detailed simulation MFD model is regarded as the plant (reality). Accordingly, a deep-learning LSTM-NN (instead of an explicit route choice model) is integrated within the prediction model to accurately estimate the percentage of inter-region transfer flows. This relaxes the requirement of destination information and homogeneity-proportionality assumption on inter-region transfer flows. Results indicate that the proposed cordon congestion pricing scheme can effectively achieve both goals by diminishing the vehicles' total time spent by 11.66% compared to the No toll scenario as well as preserving total generated toll revenue close to zero (\$0.09 per veh).

Several future research directions are envisaged. One future research direction is to address traffic networks with multiple modes. The effect of congestion pricing on the impacts of departure time choices (e.g. Yildirimoglu and Ramezani, 2020; Yildirimoglu et al., 2021; Kumarage et al., 2021) can also shed light on practical complications of field implementation. Furthermore, a research priority is to consider the income and value of time heterogeneity of travelers by differentiating user groups with assorted socio-economic features to improve the fairness and acceptability of the pricing strategies. The proposed cordon-based revenue-neutral tolling can be analyzed as a hybrid monetary-credit-based pricing scheme, in which the allocation and expenditure mechanisms of credits in day-to-day operations of the system requires further investigation and is a pressing future research direction. Another future research direction is to investigate other learning methods. Since there are spatial correlations in the dataset other than temporal dependency, the graph convolutional network (GCN) that is capable to capture the spatial correlations among data could be considered. The integration of transfer flow measurements into machine learning is also a promising research direction.

For real-time application of the proposed congestion pricing strategy in a large urban network, the computation time is essential to remain feasibly bounded. There is the issue of the transcription method (i.e., the method employed for converting the MPC optimal control problem to a nonlinear optimization problem). The combination of transcription method, type of optimization solver, MPC timestep, and system model/problem dimensions can have a significant impact on computation time (see section III.B of Sirmatel and Geroliminis (2017)). Accordingly, realizing the real-time application of the proposed learning-based MPC algorithm is a future research direction.

CRediT authorship contribution statement

Ye Li: Conceptualization, Methodology, Software, Validation, Formal analysis, Investigation, Data curation, Writing – original draft, Writing – review & editing. **Mohsen Ramezani:** Conceptualization, Methodology, Validation, Formal analysis, Investigation, Writing – original draft, Writing – review & editing, Supervision.

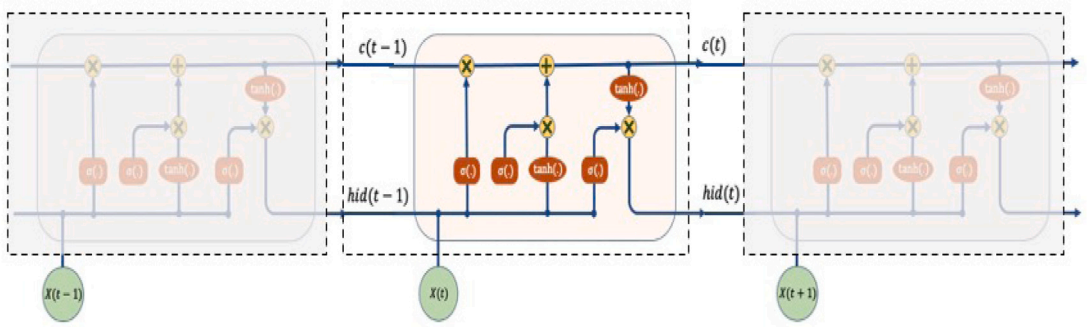

Fig. A1. Illustrations of the LSTM neural network with repeating module that allows information to be passed from one step to the next.

Appendix. The LSTM neural network

An LSTM neural network (LSTM-NN) is employed in this paper to estimate the percentage of inter-region transfer flows in the accumulation-based MFD model. LSTM-NN was originally introduced by Hochreiter and Schmidhuber (1997). The essential objective of the LSTM-NN is to overcome the limitation of the recurrent neural network (RNN) in terms of vanishing and exploding gradients when modeling the long time dependencies in time-series data. LSTM-NN is capable of learning order dependence in sequence prediction problems. The typical LSTM-NN contains three layers: input, hidden, and output layers. Different from traditional RNN, LSTM-NN includes a memory gate in the hidden layer to decide whether the information is important and necessary for prediction. Gates are composed of a sigmoid neural net and a pointwise multiplication operation, as shown in Fig. A1.

In this paper, the purpose of using LSTM-NN is to accurately estimate the percentage of transfer flows, i.e. $F_i^h(t)$ in Eq. (2). The estimated percentage of inter-region outflows will be iteratively computed by the following operations,

$$\begin{aligned} f(t) &= \sigma(W_{\mathrm{f}}^{\mathrm{T}}[hid(t-1), X(t)] + b_{\mathrm{f}}) \\ i(t) &= \sigma(W_{\mathrm{i}}^{\mathrm{T}}[hid(t-1), X(t)] + b_{\mathrm{i}}) \\ c(t) &= f(t) \odot c(t-1) + i(t) \odot \tanh(W_{\mathrm{c}}^{\mathrm{T}}[hid(t-1), X(t)] + b_{\mathrm{c}}) \\ o(t) &= \sigma(W_{\mathrm{o}}^{\mathrm{T}}[hid(t-1), X(t)] + b_{\mathrm{o}}) \\ hid(t) &= o(t) \odot \tanh(c(t)) \end{aligned} \tag{A.1}$$

where $f(t)$, $i(t)$, $c(t)$, $o(t)$, and $hid(t)$ are the forget, input, cell-state, output, and hidden state at time t, respectively; W_{f}, W_{i}, W_{o}, and W_{c} are the weight vectors for the forget, input, cell-state, and output layers; b_{f}, b_{i}, b_{o}, and b_{c} are the corresponding bias vectors; $X(t)$ is the input data at the current time t; $hid(t-1)$ represents the input received from the previous time step; $\sigma(\cdot)$ denotes the standard logistics sigmoid function; and $\odot$ represents the scalar product of two vectors.

For the prediction model presented in Eq. (1), the final output can be expressed in terms of the input (i.e. Eq. (A.1)) as:

$$\hat{Y}_i(t) = W_{\mathrm{LSTM}}^{\mathrm{T}}[hid(t-d), hid(t-(d+1)), \ldots, hid(t)] + B_{\mathrm{LSTM}} \tag{A.2}$$

where $W_{\mathrm{LSTM}}^{\mathrm{T}}$ and B_{LSTM} are weight and bias vectors.

A.1. The LSTM-NN training procedure and validation

The developed LSTM neural networks can be utilized to estimate the percentage of inter-region transfer flows (see Section 2). The estimation process begins with normalizing the historical dataset. Note that the historical dataset is obtained from simulations, while it can be easily replaced with field data. Fig. A1 exhibits the data processing module in the hidden layer of LSTM-NN. The selected variables (i.e. Eq. (3)) constitute the input vector of which utilized in the designed LSTM-NNs. Based on the input vector ($X(t)$), the LSTM-NN module can retain and transmit conducive characteristics (i.e. $c(t-1)$ and $hid(t-1)$) from previous time step to the next step.

The historical dataset used for LSTM-NN training and validation contains a total of 65 replications considering disparate pricing policies of the whole traffic simulation procedure, such as No toll, random tolls, Bang–Bang pricing (or on–off control), PI control with $\tau^{\min} = 0$, PI control with $\tau^{\min} = -\mathrm{fftt} \cdot \mathrm{VOT}$, PI control plus a random component, MPC with $\tau^{\min} = 0$ and $\alpha = 0$, and MPC with $\tau^{\min} = -\mathrm{fftt} \cdot \mathrm{VOT}$ and $\alpha = 0$. Note that the regional tolls in these replications are bounded between the corresponding minimum toll ($\tau^{\min}$) and the maximum toll (i.e. $\tau^{\max} = 5$). Also note that a variety of different demands (dissimilar from the demand in the numerical experiment) were utilized to train the LSTM-NN. In this study, the complete dataset is randomly partitioned into two parts. The first part includes 59 (90%) replications of the dataset, of which a total of 20000 time sequences were picked randomly to create the training set, and the remaining part contains 6 (10%) replications that were used for validation. LSTM-NNs in this paper were trained through Matlab (2021a version) deep-learning toolbox considering two LSTM-NN layers with 128 and 256 hidden units, respectively.

References

Daganzo, C.F., Lehe, L.J., 2015. Distance-dependent congestion pricing for downtown zones. Transp. Res. B 75, 89–99.

Chen, Y., Zheng, N., Vu, H.L., 2021. A novel urban congestion pricing scheme considering travel cost perception and level of service. Transp. Res. C 125, 103042.

Gu, Z., Saberi, M., 2021. Simulation-based optimization of toll pricing in large-scale urban networks using the network fundamental diagram: A cross-comparison of methods. Transp. Res. C 122, 102894.

Aalipour, A., Kebriaei, H., Ramezani, M., 2018. Analytical optimal solution of perimeter traffic flow control based on mfd dynamics: a pontryagin's maximum principle approach. IEEE Trans. Intell. Transp. Syst. 20 (9), 3224–3234.

Mohajerpoor, R., Saberi, M., Vu, H.L., Garoni, T.M., Ramezani, M., 2020. H_∞ robust perimeter flow control in urban networks with partial information feedback. Transp. Res. B 137, 47–73.

Li, Y., Mohajerpoor, R., Ramezani, M., 2021. Perimeter control with real-time location-varying cordon. Transp. Res. B 150, 101–120.

Sirmatel, I.I., Geroliminis, N., 2021. Stabilization of city-scale road traffic networks via macroscopic fundamental diagram-based model predictive perimeter control. Control Eng. Pract. 109, 104750.

Li, Y., Yildirimoglu, M., Ramezani, M., 2021. Robust perimeter control with cordon queues and heterogeneous transfer flows. Transp. Res. C 126, 103043.

Yildirimoglu, M., Ramezani, M., Geroliminis, N., 2015. Equilibrium analysis and route guidance in large-scale networks with MFD dynamics. Transp. Res. C 59, 404–420.

Yildirimoglu, M., Sirmatel, I.I., Geroliminis, N., 2018. Hierarchical control of heterogeneous large-scale urban road networks via path assignment and regional route guidance. Transp. Res. B 118, 106–123.

Batista, S., Leclercq, L., Menéndez, M., 2021. Dynamic traffic assignment for regional networks with traffic-dependent trip lengths and regional paths. Transp. Res. C 127, 103076.

Haddad, J., Ramezani, M., Geroliminis, N., 2013. Cooperative traffic control of a mixed network with two urban regions and a freeway. Transp. Res. B 54, 17–36.

Han, Y., Ramezani, M., Hegyi, A., Yuan, Y., Hoogendoorn, S., 2020. Hierarchical ramp metering in freeways: an aggregated modeling and control approach. Transp. Res. C 110, 1–19.

Ramezani, M., Nourinejad, M., 2018. Dynamic modeling and control of taxi services in large-scale urban networks: A macroscopic approach. Transp. Res. C 94, 203–219.

Wei, B., Saberi, M., Zhang, F., Liu, W., Waller, S.T., 2020. Modeling and managing ridesharing in a multi-modal network with an aggregate traffic representation: a doubly dynamical approach. Transp. Res. C 117, 102670.

Liu, Z., Meng, Q., Wang, S., 2013. Speed-based toll design for cordon-based congestion pricing scheme. Transp. Res. C 31, 83–98.

Zheng, N., Geroliminis, N., 2020. Area-based equitable pricing strategies for multimodal urban networks with heterogeneous users. Transp. Res. Part A: Policy Prac. 136, 357–374.

Basso, L.J., Jara-Díaz, S.R., 2012. Integrating congestion pricing, transit subsidies and mode choice. Transp. Res. Part A: Policy Prac. 46 (6), 890–900.

Zheng, N., Rérat, G., Geroliminis, N., 2016. Time-dependent area-based pricing for multimodal systems with heterogeneous users in an agent-based environment. Transp. Res. C 62, 133–148.

Amirgholy, M., Gao, H.O., 2017. Modeling the dynamics of congestion in large urban networks using the macroscopic fundamental diagram: User equilibrium, system optimum, and pricing strategies. Transp. Res. B 104, 215–237.

Kaddoura, I., Nagel, K., 2019. Congestion pricing in a real-world oriented agent-based simulation context. Res. Transp. Econ. 74, 40–51.

Godfrey, J., 1969. The mechanism of a road network. Traffic Eng Control 8 (8).

Geroliminis, N., Daganzo, C.F., 2008. Existence of urban-scale macroscopic fundamental diagrams: Some experimental findings. Transp. Res. B 42 (9), 759–770.

Gayah, V.V., Daganzo, C.F., 2011. Clockwise hysteresis loops in the macroscopic fundamental diagram: an effect of network instability. Transp. Res. B 45 (4), 643–655.

Saeedmanesh, M., Geroliminis, N., 2017. Dynamic clustering and propagation of congestion in heterogeneously congested urban traffic networks. Transp. Res. B 105.

Saedi, R., Saeedmanesh, M., Zockaie, A., Saberi, M., Geroliminis, N., Mahmassani, H.S., 2020. Estimating network travel time reliability with network partitioning. Transp. Res. C 112, 46–61.

Zheng, N., Waraich, R.A., Axhausen, K.W., Geroliminis, N., 2012. A dynamic cordon pricing scheme combining the macroscopic fundamental diagram and an agent-based traffic model. Transp. Res. Part A: Policy Prac. 46 (8), 1291–1303.

Simoni, M., Pel, A., Waraich, R.A., Hoogendoorn, S., 2015. Marginal cost congestion pricing based on the network fundamental diagram. Transp. Res. C 56, 221–238.

Chen, X.M., Xiong, C., He, X., Zhu, Z., Zhang, L., 2016. Time-of-day vehicle mileage fees for congestion mitigation and revenue generation: A simulation-based optimization method and its real-world application. Transp. Res. C 63, 71–95.

Dantsuji, T., Fukuda, D., Zheng, N., 2019. Simulation-based joint optimization framework for congestion mitigation in multimodal urban network: a macroscopic approach. Transportation 1–25.

Jakob, M., Menendez, M., 2021. Parking pricing vs. congestion pricing: a macroscopic analysis of their impact on traffic. Transp. A: Transp. Sci. 17 (4), 462–491.

Genser, A., Kouvelas, A., 2022. Dynamic optimal congestion pricing in multi-region urban networks by application of a multi-layer-neural network. Transp. Res. C 134, 103485.

Gu, Z., Liu, Z., Cheng, Q., Saberi, M., 2018. Congestion pricing practices and public acceptance: A review of evidence. Case Stud. Transp. Policy 6 (1), 94–101.

Lehe, L., 2019. Downtown congestion pricing in practice. Transp. Res. C 100, 200–223.

Schuitema, G., Steg, L., Forward, S., 2010. Explaining differences in acceptability before and acceptance after the implementation of a congestion charge in stockholm. Transp. Res. Part A: Policy Prac. 44 (2), 99–109.

Levinson, D., 2010. Equity effects of road pricing: A review. Transp. Rev. 30 (1), 33–57.

Arnott, R., De Palma, A., Lindsey, R., 1994. The welfare effects of congestion tolls with heterogeneous commuters. J. Transp. Econ. Policy 139–161.

Kristoffersson, I., Engelson, L., Börjesson, M., 2017. Efficiency vs equity: Conflicting objectives of congestion charges. Transp. Policy 60, 99–107.

Liu, Y., Guo, X., Yang, H., 2009. Pareto-improving and revenue-neutral congestion pricing schemes in two-mode traffic networks. NETNOMICS: Econ. Res. Electron. Netw. 10 (1), 123–140.

Yang, H., Wang, X., 2011. Managing network mobility with tradable credits. Transp. Res. B 45 (3), 580–594.

Adler, J.L., Cetin, M., 2001. A direct redistribution model of congestion pricing. Transp. Res. B 35 (5), 447–460.

Geroliminis, N., Haddad, J., Ramezani, M., 2012. Optimal perimeter control for two urban regions with macroscopic fundamental diagrams: A model predictive approach. IEEE Trans. Intell. Transp. Syst. 14 (1), 348–359.

Ramezani, M., Haddad, J., Geroliminis, N., 2015. Dynamics of heterogeneity in urban networks: Aggregated traffic modeling and hierarchical control. Transp. Res. B 74, 1–19.

Csikós, A., Charalambous, T., Farhadi, H., Kulcsár, B., Wymeersch, H., 2017. Network traffic flow optimization under performance constraints. Transp. Res. C 83, 120–133.

Batista, S.F., Ingole, D., Leclercq, L., Menéndez, M., 2021. The role of trip lengths calibration in model-based perimeter control strategies. IEEE Trans. Intell. Transp. Syst..

Menelaou, C., Timotheou, S., Kolios, P., Panayiotou, C.G., 2021. Joint route guidance and demand management for real-time control of multi-regional traffic networks. IEEE Trans. Intell. Transp. Syst..

Jiang, X., Zhang, L., Chen, X.M., 2014. Short-term forecasting of high-speed rail demand: A hybrid approach combining ensemble empirical mode decomposition and gray support vector machine with real-world applications in China. Transp. Res. C 44, 110–127.

Wu, Y., Tan, H., Qin, L., Ran, B., Jiang, Z., 2018. A hybrid deep learning based traffic flow prediction method and its understanding. Transp. Res. C 90, 166–180.

Ma, X., Tao, Z., Wang, Y., Yu, H., Wang, Y., 2015. Long short-term memory neural network for traffic speed prediction using remote microwave sensor data. Transp. Res. C 54, 187–197.

Gu, Y., Lu, W., Qin, L., Li, M., Shao, Z., 2019. Short-term prediction of lane-level traffic speeds: A fusion deep learning model. Transp. Res. C 106, 1–16.

Sirmatel, I.I., Tsitsokas, D., Kouvelas, A., Geroliminis, N., 2021. Modeling, estimation, and control in large-scale urban road networks with remaining travel distance dynamics. Transp. Res. C 128, 103157.

Liu, W., Geroliminis, N., 2017. Doubly dynamics for multi-modal networks with park-and-ride and adaptive pricing. Transp. Res. B 102, 162–179.

Ingole, D., Mariotte, G., Leclercq, L., 2020. Perimeter gating control and citywide dynamic user equilibrium: a macroscopic modeling framework. Transp. Res. C 111, 22–49.

Cui, Z., Ke, R., Pu, Z., Wang, Y., 2020. Stacked bidirectional and unidirectional LSTM recurrent neural network for forecasting network-wide traffic state with missing values. Transp. Res. C 118, 102674.

Roy, K.C., Hasan, S., Culotta, A., Eluru, N., 2021. Predicting traffic demand during hurricane evacuation using real-time data from transportation systems and social media. Transp. Res. C 131, 103339.

Sun, J., Kim, J., 2021. Joint prediction of next location and travel time from urban vehicle trajectories using long short-term memory neural networks. Transp. Res. C 128, 103114.

Mariotte, G., Leclercq, L., Laval, J.A., 2017. Macroscopic urban dynamics: Analytical and numerical comparisons of existing models. Transp. Res. B 101, 245–267.

Yildirimoglu, M., Ramezani, M., 2020. Demand management with limited cooperation among travellers: A doubly dynamic approach. Transp. Res. B 132, 267–284.

Yildirimoglu, M., Ramezani, M., Amirgholy, M., 2021. Staggered work schedules for congestion mitigation: A morning commute problem. Transp. Res. C 132, 103391.

Kumarage, S., Yildirimoglu, M., Ramezani, M., Zheng, Z., 2021. Schedule-constrained demand management in two-region urban networks. Transp. Sci. 55 (4), 857–882.

Sirmatel, I.I., Geroliminis, N., 2017. Economic model predictive control of large-scale urban road networks via perimeter control and regional route guidance. IEEE Trans. Intell. Transp. Syst. 19 (4), 1112–1121.

Hochreiter, S., Schmidhuber, J., 1997. Long short-term memory. Neural Comput. 9 (8), 1735–1780.